Reflooding with internal boiling of a heating model porous medium with mm-scale pores

P. Sapin[a,b], A. Gourbil[a,b], P. Duru[a,*], F. Fichot[b], M. Prat[a,c], M. Quintard[a,c]

[a] *Université de Toulouse; INPT, UPS; IMFT (Institut de Mécanique des Fluides de Toulouse); Allée Camille Soula, F-31400 Toulouse, France.*
[b] *Institut de Radioprotection et de Sûreté Nucléaire (IRSN), Division of Major Accidents Prevention, BP3 13115 St Paul lez Durance, France.*
[c] *CNRS ; IMFT ; F-31400 Toulouse, France.*

Abstract

This paper presents a pore-scale experimental study of the reflooding of a two-dimensional model porous medium. The objective is to better understand the reflooding mechanisms in play in the context of nuclear reactor safety. The hot debris bed that forms in a nuclear reactor following a loss of coolant accident is comparable to a heat-generating porous medium. Its cooling by water reflooding involves intense boiling mechanisms that must be modeled properly to assess mitigation procedures

The experimental study presented in this paper focuses on the phenomenology of reflooding of a model porous medium composed of a bank of mm-scale heating cylinders randomly placed between two ceramic plates. A Fluorinert^{TM} liquid, HFE-7000, is injected at a temperature close to saturation into the dry and superheated porous medium. Each cylinder of the test section is used both as a heating element and a temperature probe,

*Corresponding author.
Email address: paul.duru@imft.fr (P. Duru)

which enables to track the evolution of the three different macroscopic zones identified during cooling of the system. The reflooding dynamics, in particular the cooling fronts velocities, are thus determined thanks to pore-scale thermal measurements together with direct visualizations. The influence of the injection flow rate and of the heating power are studied in a parametric way.

Keywords:

Nuclear safety, Hot debris bed, Boiling, Porous media.

Nomenclature

d_c	Cylinder diameter (RTD probe diameter), m.
d_p	Diameter of the particles formed by the collapse of fuel rods, m.
ε	Porosity, $-$.
G_l	Flow rate, m^3/s.
L_{cap}	Capillary length, m.
Q	Heating power per cylinder, W.
S	Setup cross-section area, m^2.
t_c	Time when a cylinder is said to be reflooded or cooled down, s.
t_{qf}	Time of arrival of the quenching front, s.
T_{inj}	Inlet temperature, °C.
T_{sat}	Saturation temperature, °C.
v_l	Intrinsic liquid velocity, m/s.
v_{qf}	Velocity of the quenching front, m/s.
v_c	Velocity of the cooling front, m/s.

$y_c{}^{th}$	Position of the cooling front in the y-direction deduced from thermal measurements, m.
y_{qf}	Position of the quenching front in the y-direction, m.
$y_{qf}{}^{th}$	Position of the quenching front in the y-direction deduced from thermal measurements, m.

1. Introduction

Two-phase flows in porous media with liquid-vapor phase change are involved in various systems covering, for example, fuel cells [1], heat pipes [2], geothermal reservoirs [3] and severely degraded cores of nuclear reactors [4, 5], the case of interest related to the present study.

In the aftermath of a loss of coolant accident (LOCA scenario), residual decay heat in a nuclear reactor core can cause dry-out of water in the vessel, destruction of fuel rods and melting of core materials, thus creating a molten pool commonly called *corium*. To prevent the spread of molten materials, the reactor vessel can be cooled down by reflooding with water. Yet, quenching of very hot rods in the upper plenum may result in their collapse, thus forming a *debris bed* heated up by residual decay heat, comparable to a highly permeable porous medium: the typical particle size, d_p, is in the range $1-10\,\mathrm{mm}$, which is of the same order of magnitude than the water capillary length L_{cap}. Reflooding of this dry and heat-generating porous medium is a crucial step in the cooling process. Indeed, a non-coolable particle bed

might melt down, thus expanding the *corium* pool and possibly damaging the reactor vessel.

In terms of nuclear safety analysis, intense boiling mechanisms and complex flow regimes encountered at the pore scale in the debris bed must be modeled properly to estimate the efficiency of the reflooding and to assess mitigation procedures in case of such severe accident. A classical modeling approach consists in describing this complex three-phase system (two-phase cross-flow with liquid-vapor phase change within a packed particle bed) at a macroscopic scale by introducing equivalent continuous media, whose properties at each point are effective transport properties representative of the pore-scale configuration, and to write down conservation equations. Thermal inertia of the particles, important convective heat transfers and rapid evaporation processes are responsible for significant local differences between the three phase-averaged temperatures defined for the solid, liquid and gas phases. Such a local thermal non-equilibrium situation requires the introduction of separate energy equations for the different phases. Duval *et al.* [6] derived macroscopic equations from the local energy and mass conservation laws with the volume averaging method [7]. They obtained macroscopic laws for the gas, liquid and solid phases, accounting for diffusion, convection and evaporation contributions. Providing explicit relations between the effective properties of the macroscopic model and the pore-scale configuration requires to write local closure problems to be solved over representative unit cells.

So far, such effective properties have been determined analytically for very simple unit cells, considering two main configurations: stratified solid-liquid-gas (SLG, where liquid is the wetting phase) or solid-gas-liquid (SGL, where

gas is the wetting phase) flows, this latter configuration being reminiscent of a film boiling situation. These simple calculations emphasized the strong impact of the phase repartition upon the effective properties.

However, practical application to convective boiling problems in porous media faces a major difficulty. Boiling phenomenons lead to various, often highly transient, liquid-gas repartitions, especially at the solid-fluids interface where both liquid and gas can wet the solid surface. Heterogeneous nucleation and coalescence of bubbles are indeed complex processes that can hardly be described by stratified configurations with static interfaces, such as SLG or SGL configurations.

Comprehensive approaches have already been proposed to predict heat exchanges in boiling configurations and successfully compared to experimental data obtained on micro-fabricated surfaces. For instance, studies by Liter and Kaviany [8] and Dhir [9, 10] allow to be optimistic that comprehensive models would be able to estimate boiling heat transfer in complex configurations. However, to our knowledge, no correlation is currently available to estimate the convective boiling contribution to heat exchanges during reflooding of a porous medium. Bachrata *el al.* [11] thus proposed a semi-heuristic approach that consists of adding heat source terms into the solid energy equation of Duval *et al.*'s model [6] to account for nucleate, transition and film boiling contributions, with empirical or mechanism-based correlations. The key challenge of such a solution is to choose adapted correlations, because of the numerous influential parameters. In particular, Kew and Cornwell [12], Thome [13] and Cheng and Wu [14] outlined the strong effect of confinement on boiling phenomenology and on the resulting heat transfer coefficient. And

with any of the transition criteria proposed in these studies, the different characteristic flow paths in the concerned packed debris beds can be classified as either macroscale, mesoscale and microscale channels with respect to two-phase processes (considering vapour and liquid water).

It is thus essential to obtain pore-scale visualization about phase distribution that will help either:
– to estimate effective transport properties in more realistic representative unit cells, and/or
– to choose more carefully convective boiling correlations for heuristic or semi-heuristic approaches.

Such information was not obtained in previous experimental studies of reflooding of superheated porous structures, a subject investigated experimentally since the 1980s ([15, 16, 17, 18]). In fact, such studies are typically performed on 3D packing of superheated beads, preventing any visualization at pore scale. They aim primarily at obtaining data at macroscopic scale (pressure, global vapor production,...) that can be used to adjust parameters of some macroscopic models (see, e.g., the insights obtained from Repetto *et al.* [19], Bachrata *et al.* [11] and Fichot *et al.*'s [20] experimental studies on Duval *et al.*'s modeling [6]).

In the following, the experimental setup and techniques used in the present study to obtain visualizations and thermal measurements during reflooding of a model porous medium are first presented. They aim at obtaining results at the pore scale and also allow to characterize the dynamic of reflooding at a macroscopic level by identifying the different flow regimes. Such results are detailed in Section 3. Conclusions are then drawn in Section 4.

2. Experimental setup and measurement techniques

2.1. Experimental setup

The experimental test section consists of a nearly two-dimensional porous medium made of 392 cylinders placed between two parallel ceramic plates and held vertically, see Figure 1. The spacing between the two plates is 3 mm. The 2.1 mm diameter cylinders are positioned in a slightly randomly-disturbed staggered arrangement that spans the setup width (50 mm) and extends over a 80 mm height. The resulting porosity is then $\varepsilon = 0.65$. The two plates are respectively a Macor$^{\text{TM}}$ ceramic plate and a polished,

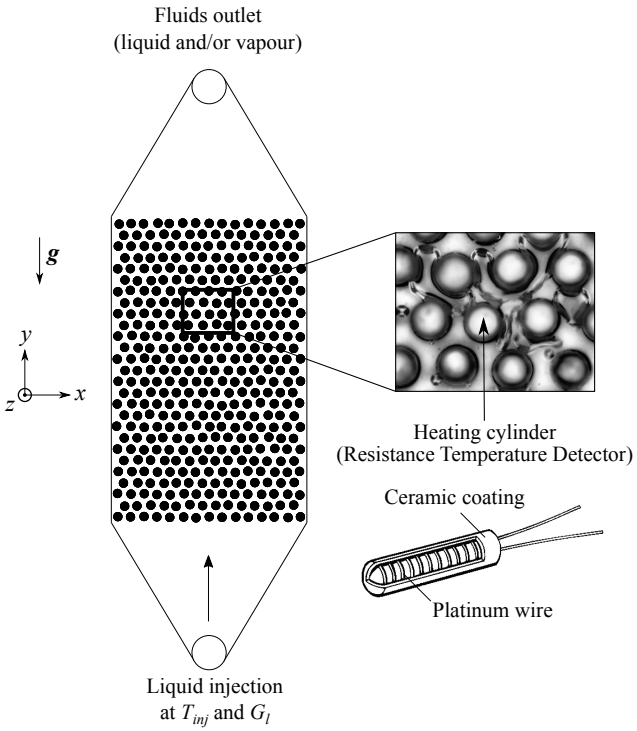


Figure 1: Sketch of the experimental test section: a "two-dimensional" model porous medium. Each cylinder is a platinum resistance temperature detector.

transparent Vycor® glass plate which seals the test section while allowing visualization. These materials have been chosen because of their ability to withstand high temperatures. The porous section is preceded by a divergent part to obtain a flat liquid injection front. The two-phase mixture exits at the top of the test section.

The key feature of the experimental test section lies in the fact that each cylinder is a resistance temperature detector (RTD) composed of a coiled platinum wire wrapped around an insulating core, sealed into a 2.1 mm diameter and 7 mm long ceramic coating (see Figure 1). Each RTD is used as a heating element but also as a local temperature probe, as explained in subsection 2.2.1. Note that the smaller size of the heating cylinders and their strong confinement between the two ceramic plates are two major differences with typical tube bundle geometries, for which convective boiling has been studied experimentally since the early 1950s (see, e.g., [21, 22, 23]).

HFE-7000 was chosen as the working fluid because of its low saturation temperature ($T_{sat} = 34\,^{\circ}\mathrm{C}$ at atmospheric pressure). Reflooding experiments can then be run with moderate thermal constraints. In addition, this Fluorinert™ fluid is non-toxic, non-flammable and dielectric, which guarantees safety during handling. HFE-7000 perfectly wets the ceramic surfaces it is in contact with (contact angle close to 0°). Also, it is worth mentioning that the ratio of the capillary length of HFE-7000 to the diameter of the cylindrical heating elements is similar to the one obtained when considering the ratio between the capillary length of water at 100 °C and a characteristic 5 mm particle size, typical of the one observed in debris bed. Indeed, observations of the damaged TMI-2 reactor [24] and different experimental studies

(see, e.g., the TMI-2 core sample examinations by McCardell *et al.* [25], the LOFT experiment analysis by Coryell *et al.* [26], and the microscopic observations of fuel samples made by Manzel and Walker [27]) characterized the particles formed by the collapse of fuel rods: their size d_p approximately lies between 1 and 10 mm. Thus, realistic boiling conditions are obtained in the present experimental setup, as far as bubble size and confinement effects are concerned.

The fluid flow is driven by a gear pump (see Figure 2(a)), the head of which is composed of stainless steel with PTFE teeth. The pump thus requires no lubrication and this cancels the risk of HFE-7000 contamination by a lubricating fluid. The fluid temperature is controlled by circulation through a coil immersed in a constant temperature bath. Inlet temperature T_{inj} and flow rate G_l are measured upstream of the test section. For the experiments reported in the present paper, the fluid was injected at a temperature close

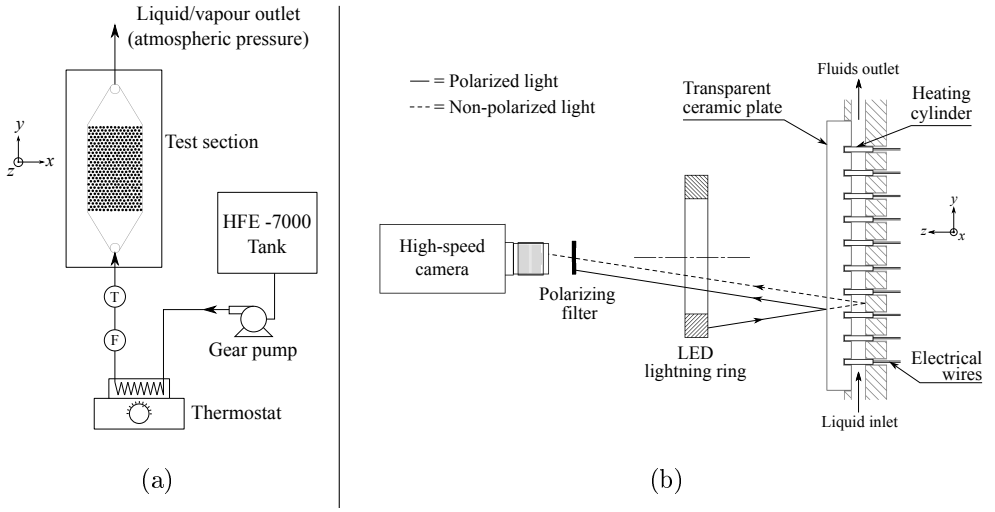


Figure 2: (a) Experimental setup: an open fluid circuit. (b) Side view of the test section, showing the visualization configuration.

to its saturation temperature ($T_{inj} \approx T_{sat}$). The intrinsic injection velocity v_l is obtained by dividing the imposed flow rate by the product of the setup cross-section S ($3 \times 50\,\mathrm{mm}^2$) times the porosity ε:

$$v_l = \frac{G_l}{\varepsilon S}. \tag{1}$$

In the present study, using v_l rather than the flow rate G_l is more relevant as v_l is the theoretical average rising velocity of the liquid front in the test section, in the absence of phase change.

2.2. Experimental techniques

2.2.1. Thermal control, temperature measurements and direct visualizations

The electrical resistance of each RTD ($100\,\Omega$ at $0\,^\circ\mathrm{C}$) varies with temperature according to a well-known law. RTDs are classically used with very low currents to measure resistance, and thus temperature, while avoiding self-heating. Whereas Joule effect is usually considered as a source of error, RTDs are used here both as heating elements and as local temperature probes. However, the dependence of resistance upon temperature leads to an additional challenge. In order to control the heating power transmitted to each cylinder, the voltage applied at the ends of each resistive wire must be adjusted continuously. All heating cylinders are connected to a stabilized power supply through a control module comprising a proportional-integral controller equipped with a 1000 Hz micro-processor. Each RTD therefore dissipates a well-controlled heat flux while its temperature is recorded at a very high acquisition rate.

Insights on the liquid and vapor phases distribution during a reflooding experiment are obtained by direct visualization performed using a PCO Di-

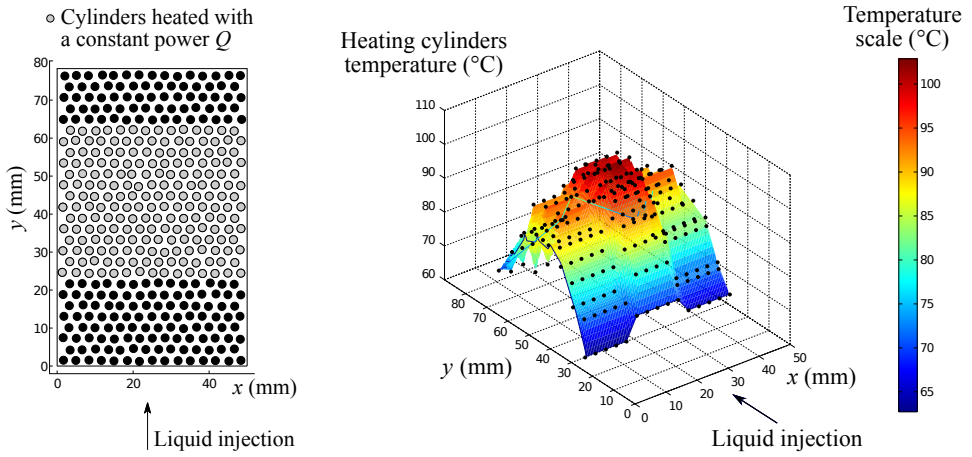
max high-speed camera. The frame acquisition rate is typically around 250 frames per second, with a low exposure time (1 ms) to avoid motion blur. A white LEDs ring providing a polarized light is placed in front of the transparent ceramic plate and aligned with the CCD (charge-coupled device) camera optical axis, see Figure 2(b). This optical configuration limits the shadowing effect due to the many close cylinders that would have been obtained with a lighting from the side. Also, the amount of light that is simply reflected at the surface of the transparent ceramic plate is removed by a polarizing filter. This layout enables to achieve a nearly homogeneous lighting of the test section.

2.2.2. Protocol for a reflooding experiment

Reflooding experiments are performed on an uniformly heated model porous medium. The constant heating power applied to each cylinder, Q, and the liquid injection velocity, v_l, are the two experimental control parameters. The protocol for a reflooding experiment is the following.

First, the HFE-7000 tank is closed and a vacuum pump is connected at the top of the dry test section, to extract air from the whole fluid circuit. HFE-7000 tank is then opened so that the full system fills gently with liquid. This procedure aims at limiting the amount of air remaining trapped in the system. Second, a heating power is applied to the cylinders to dry the model porous medium while the test section top is opened at atmospheric pressure to avoid any pressure build-up. Finally, liquid is injected with a velocity v_l in the dry porous medium saturated with HFE-7000 vapor and heated with a constant thermal power.

It is important to note that only a fraction of the bundle of cylinders is



(a) (b)

Figure 3: (a) Heating configuration of the model porous medium used in the reflooding experiments. (b) Initial steady-state temperature profile of the heated part of the dry porous medium ($Q = 80\,\mathrm{mW}$).

heated during a reflooding experiment, typically 14 rows of cylinders (203 cylinders) in the middle of the test section, see Figure 3(a). While limiting the total electric power to be delivered to the electronic control units, this is enough as measurements are then performed in a region of the system where the influence of entry and exit effects can be neglected (that is, respectively, establishment of the flow field in the porous bed, and flow recirculation in the top converging part of the test section, the influence of which extends over the very last rows of the test section).

A typical initial steady-state temperature profile is shown in Figure 3(b) for a heating power $Q = 80\,\mathrm{mW}$ per element. The observed thermal gradients are due to heat losses towards the side plates (ceramic) around the cylinder bundle, to heat conduction in those plates and to natural convection with air outside of the test section.

3. Experimental results

3.1. Two-phase flow configuration and temperature distribution

We first describe qualitatively the two-phase flow configuration typically observed in a reflooding experiment. Figure 4 shows an image taken once the liquid has reached the heated porous region. From top to bottom, three distinct zones can be observed. First, a single-phase vapor zone with some isolated liquid droplets ejected from the intense boiling zone. Second, an intense boiling zone where coalescence of bubbles is very frequent so that one can hardly discern any flow pattern. And finally, a nucleate boiling zone where vapor bubbles can be clearly visualized. A fourth zone corresponding to a one-phase liquid flow could be observed in such experiments if the subcooling of the fluid was higher. This condition was not fulfilled for this experiment because the liquid enters almost at saturation temperature.

Such a two-phase flow configuration leads us to define a quenching front

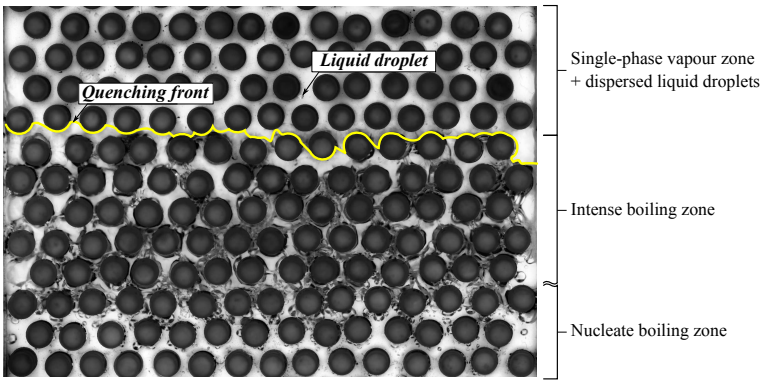


Figure 4: Visualization of the two-phase flow configuration during reflooding. In this experiment, the porous medium was heated with a constant heating power $Q = 80\,\mathrm{mW}$ and the liquid injected at a velocity $v_l = 3.6\,\mathrm{mm/s}$.

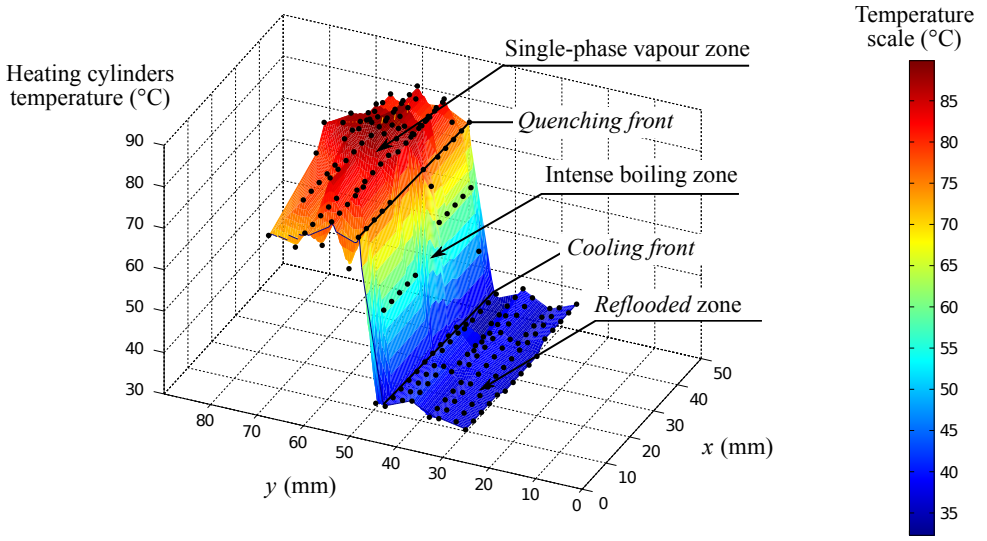


Figure 5: Instantaneous temperature spatial distribution during reflooding, at a time corresponding to the two-phase flow distribution shown in Figure 4.

separating the two first zones (it is highlighted as a clear line in Figure 4), and a cooling front separating the two last ones, that is difficult to detect precisely from visualizations. Instantaneous temperature distribution at the test section scale confirms the relevance of such a description, see Figure 5. It is noticeable that despite the high permeability of the porous medium, the thermal gradients in the initial temperature profile (Figure 3(b)) and the higher permeability at the lateral sides of the cylinder bundle, macroscopic behavior during a reflooding experiment turns out to be very close to a one-dimensional configuration with flat quenching and cooling fronts and very low thermal gradients in the x-direction. Consequently, quantitative information about the two fronts displacements can be obtained by focusing on the temperature evolution recorded for each heating element.

Figure 6 displays a typical temperature *vs* time signal obtained for a single

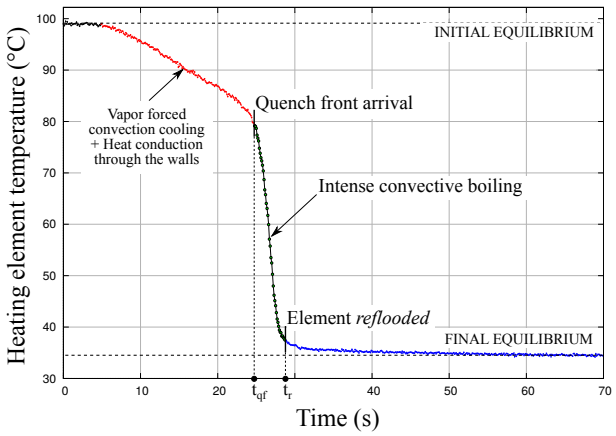


Figure 6: Temperature evolution of a heating element during reflooding.

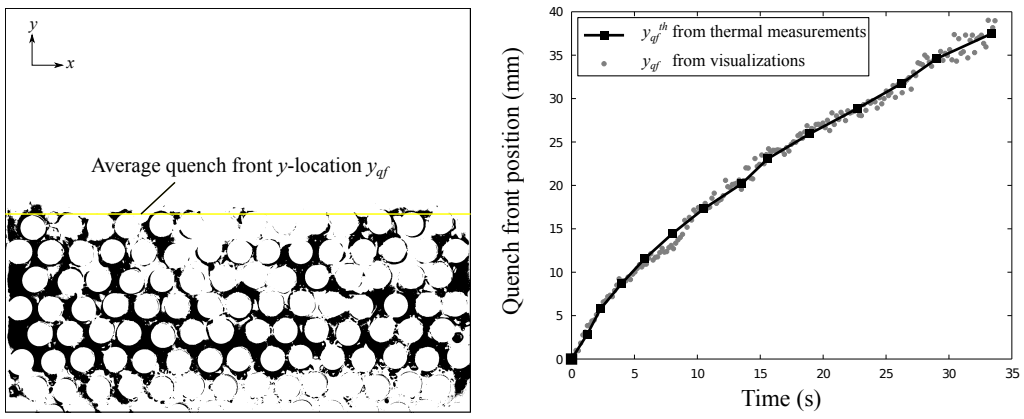
central heating cylinder. Once reflooding starts, a significant temperature decrease is observed. The local thermal non-equilibrium between the vapor phase and the superheated solid is not the only reason for the solid element temperature decrease downstream of the quenching front. It is partly due to the forced convection associated with the vapor flow generated in the zone upstream from the quenching front, but also to heat conduction through the ceramic walls. At a time noted t_{qf} ($t_{qf} = 24.8\,\mathrm{s}$ in Figure 6), the heat flux extracted from the heating element increases abruptly. Eventually, the cylinder is considered to be reflooded – or cooled down – at t_c, when a permanent nucleate boiling regime is reached around it (note that a reflooded cylinder still produces vapor because the heat flux supplied to it is maintained constant during the experiment at a sufficiently high level to cause boiling).

3.2. Quenching and cooling fronts detection

Relating the arrival of the quenching front at the y-location of the considered heating element to the temperature drop observed at t_{qf} is *a priori*

not straightforward. Heat diffusion through the walls and thermal inertia of the cylinders might induce a delay between the actual position of the two-phase front y_{qf} and the position obtained from thermal measurements ${y_{qf}}^{th}$ (deduced from the time t_{qf} associated with the discrete spatial y-location of each cylinder). Indeed, the response time of a RTD probe is approximately 0.4 s, which is not negligible with respect to the cooling duration of a heating element ($t_{qf} - t_c = 4\,\mathrm{s}$ in this example).

The position of the quenching front y_{qf} can be obtained unambiguously by processing the image sequence given by the high-speed camera. After detection of the cylinders, a mask is created in order to isolate the pore space. A background is then subtracted from each image of the sequence and a canny



(a) (b)

Figure 7: (a) Binary image used to detect the quenching front location, obtained after processing of the image shown in Figure 4. For each column of the image, the location of the uppermost black pixel is automatically detected. Then, an average is performed along the full width of the image to obtain y_{qf} (shown as a yellow solid line). (b) Temporal evolution of the quenching front location obtained from temperature measurements (filled black squares) and image processing (grey dots).

filter is used to enhance edges (i.e. liquid-vapor interfaces in the present case). Binary images are finally generated, from which an average quenching front y-location can be obtained, see Figure 7(a). In Figure 7(b), the temporal evolution of y_{qf} obtained through image processing (grey dots) is compared with that of the position ${y_{qf}}^{th}$ derived from thermal measurements (filled black squares). The match between these two plots shows that the break in slope observed at t_{qf} in Figure 6 truly corresponds to the arrival of the quenching front.

With regard to the cooling front, its location is obtained from thermal measurements only, ${y_c}^{th}$ being deduced from the time t_c associated with the discrete spatial y-location of each cylinder.

Finally, temperature measurements can be used with confidence to track the spatial evolution of the quenching and cooling fronts locations, by determining the characteristic times t_{qf} and t_c for each of the heated cylinders.

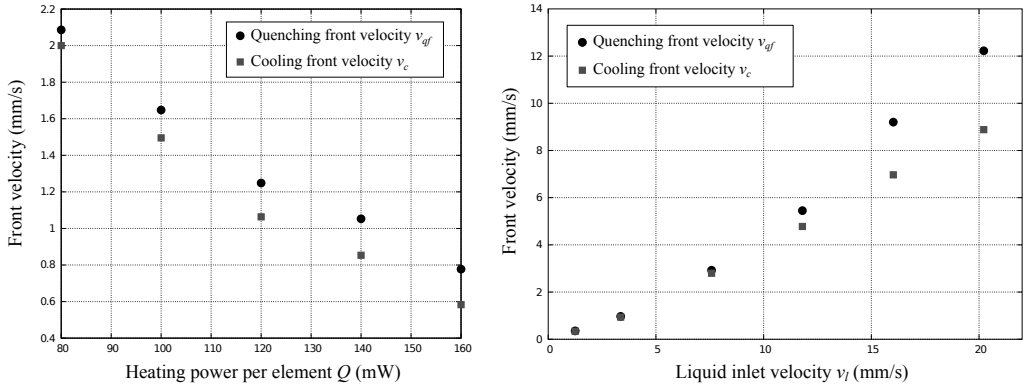
3.3. Parametric study of the quenching and cooling fronts velocities

As discussed above, tracking the locations of both the cooling and quenching fronts is made possible by the analysis of the temperature evolution of heating elements. As shown in Figure 7(b), y_{qf} increases linearly with time as soon as the quenching front has traveled over the vertical extent of a couple of rows of heating elements. A similar observation can be made for the evolution of the cooling front location y_c. Therefore, obtaining the constant quenching and cooling front velocities v_{qf} and v_c is straightforward.

These two fronts velocities are plotted in Figure 8(a) as a function of the heating power Q applied to each heating element, for a constant liquid injection velocity $v_l = 5.47\,\mathrm{mm/s}$. Increasing the heating power Q results in

larger amount of energy to be extracted by the two-phase quenching zone, which in turn induces a decrease in the fronts velocities, as expected. The very important decrease observed in Figure 8(a) suggests that it may be possible to reach a stationary regime for which the fronts would remain stationary. However, for the experiment performed with $Q = 160\,\mathrm{mW}$, the initial temperatures in the cylinders reach $\approx 200\,^{\circ}\mathrm{C}$. Heating up further would threaten the integrity of the epoxy resins used to seal the RTD probes into the Macor$^{\mathrm{TM}}$ plate (see Figure 2(b)). Therefore, it was not possible to study higher power levels.

The fronts velocities are then plotted as a function of the liquid injection velocity v_l for a fixed heating power $Q = 80\,\mathrm{mW}$, see Figure 8(b). As expected, increasing the liquid inlet velocity causes the fronts velocities to increase as well. It is worth noting that the higher v_l, the more important the difference between v_{qf} and v_c is. This result shows that the size of the intense



(a) (b)

Figure 8: (a) Influence of the heating power Q on the fronts velocities ($v_l = 5.47\,\mathrm{mm/s}$ constant). (b) Influence of liquid injection velocity v_l on the fronts velocities ($Q = 80\,\mathrm{mW}$).

boiling zone is constant for small flow rates, while it increases significantly with time for larger flow rates.

This is shown in Figure 9, for the different injection velocities investigated. On each single curve, three distinct periods can be observed. The first period, during which the size of the intense boiling zone rapidly increases, corresponds to the ingress of the quenching front into the superheated test section. Once the first bottom elements of the heated part of the test section are cooled down and have reached a steady-state nucleate boiling regime, a cooling front propagates as well within the bank of cylinders, which induces the first change in slope observed on each curve. Then, both a cooling and a quenching front can be detected in the heated part of the test section, as explained above. For small liquid injection velocities ($v_l = 1.25$ and 3.36 mm/s), the extent of the intense boiling zone does not vary much with time as v_{qf} and v_c are very close to each other (see Figure8(b)), while it

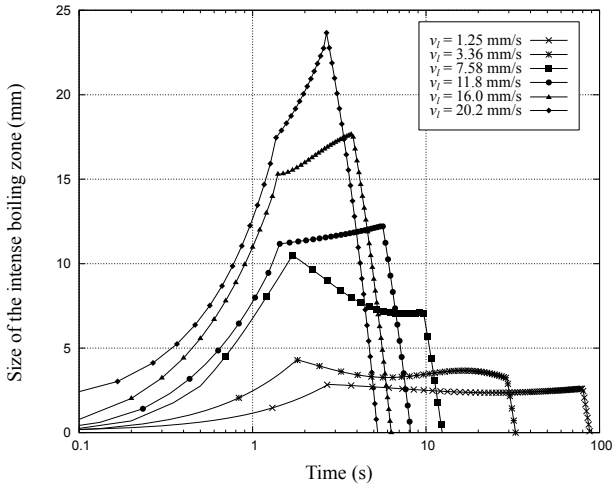


Figure 9: Size of the intense boiling zone.

significantly increases along the reflooding experiments with more important flow rates. This result is similar to the observations made on 3D column packed beds such as PRELUDE facility [19]. Finally, the size of the intense boiling zone diminishes once the quenching front has reached the upper limit of the heated part of the test section, until the cooling front reaches this limit as well.

4. Conclusion and perspectives

The experimental setup described in this article has been developed to study reflooding with internal boiling of a heating model porous medium with mm-scale pores. The main objective is to provide precise data both at the pore and macroscopic scales, with a perspective to better understand two-phase flows in porous media with intense liquid-vapor phase change. The main element of the apparatus is a slightly disordered bundle of cylinders placed between two plates, thus forming a nearly two-dimensional particle bed. Each constitutive element is a cylindrical RTD, used both as a temperature probe and a heating element. An interactive electronic device allows real-time control of the heating power transferred to each cylinder.

Close observation of the reflooding experiments enabled to identify three distinct macroscopic zones and to determine the corresponding two-phase flow regimes. In the hot vapor-dominated zone with dispersed small liquid droplets, the solid matrix is mainly cooled down by vapor forced convection and by conduction through the walls. Upstream of the quenching front, the major amount of heat is extracted in the intense boiling zone, where coalescence is so important that vapour slugs are formed, which is reminiscent

of microscopic boiling phenomenology. Finally, in the thermally established reflooded zone, classical convective nucleate boiling with isolated nucleation sites is observed.

Thermal measurements enabled to measure the quenching and cooling fronts velocities for different heating powers and injection flow rates. This parametric study shows that the macroscopic behavior and the reflooding dynamics in this model porous medium are very similar to those observed in 3D particle beds. That reinforces the proposed idea that the observations made on this test section are representative of the physics of two-phase flows in debris beds with internal boiling. The experimental setup, as well as the already obtained results, may therefore be very useful to develop more accurate pore-scale or macro-scale models and hence improve nuclear safety analysis or any other application in which intense boiling in porous media plays a major role.

In this paper, reflooding experiments were performed on a uniformly heated bank of cylinders. However, since all RTDs can be controlled individually, this setup can be used to study the influence of heterogeneous heating and the impact of a time-dependent heating power Q, situations that one may encounter in practice, for instance in the context of nuclear reactor severe accidents. This will be the subject of future studies. Furthermore, image processing techniques are currently being developed to estimate the local void fraction field from the high speed visualizations, which would provide the necessary data for subsequent quantitative modeling analysis.

Acknowledgments

Authors are particularly grateful to Ruddy Soeparno who contributed to the technical design and realization of the experimental setup and to Hervé Ayroles who built the electronic modules controlling the RTDs. Thanks also go to Electricité de France (EDF) for funding this research project.

References

[1] A. Bazylak, Liquid water visualization in PEM fuel cells: a review, International Journal of Hydrogen Energy 34 (9) (2009) 3845–3857.

[2] C. Louriou, M. Prat, Pore network study of bubble growth by vaporisation in a porous medium heated laterally, International Journal of Thermal Sciences 52 (2012) 8–21.

[3] A. Woods, Liquid and vapor flow in superheated rocks, Annual Review of Fluid Mechanics 31 (1) (1999) 171–199.

[4] G. Petrangeli, Nuclear safety, Butterworth-Heinemann, 2006.

[5] J. Libmann, Elements of nuclear safety, EDP Sciences, 2012.

[6] F. Duval, F. Fichot, M. Quintard, A local thermal non-equilibrium model for two-phase flows with phase-change in porous media, International Journal of Heat and Mass Transfer 47 (3) (2004) 613–639.

[7] S. Whitaker, The method of volume averaging, Vol. 13, Springer Netherlands, 1999.

[8] S. Liter, M. Kaviany, Pool-boiling CHF enhancement by modulated porous-layer coating: theory and experiment, International Journal of Heat and Mass Transfer 44 (22) (2001) 4287–4311.

[9] V. Dhir, Boiling heat transfer, Annual review of fluid mechanics 30 (1) (1998) 365–401.

[10] V. Dhir, Mechanistic prediction of nucleate boiling heat transfer–achievable or a hopeless task?, Journal of Heat Transfer 128 (1) (2006) 1–12.

[11] A. Bachrata, F. Fichot, G. Repetto, M. Quintard, J. Fleurot, Quench front progression in a superheated porous medium: experimental analysis and model development, Journal of Energy and Power Engineering 7 (2013) 514–523.

[12] P. Kew, K. Cornwell, Correlations for the prediction of boiling heat transfer in small-diameter channels, Applied Thermal Engineering 17 (8-10) (1997) 705–715.

[13] J. Thome, Boiling in microchannels: a review of experiment and theory, International Journal of Heat and Fluid Flow 25 (2) (2004) 128–139.

[14] P. Cheng, H. Wu, Mesoscale and microscale phase-change heat transfer, Vol. 39 of Advances in Heat Transfer, Elsevier, 2006, pp. 461 – 563.

[15] T. Ginsberg, J. Klein, C. Schwarz, J. Klages, Transient core debris bed heat removal experiments and analysis, in: International Meeting on Thermal Nuclear Reactor Safety, 1982.

[16] M. Rashid, R. Kulenovic, E. Laurien, Experimental results on the coolability of a debris bed with down comer configurations, Nuclear Engineering and Design 249 (0) (2012) 104 – 110.

[17] N. Tutu, T. Ginsberg, J. Klein, J. Klages, C. Schwarz, Debris bed quenching under bottom flood conditions, Technical Report, Brookhaven National Laboratory, Upton, New York.

[18] C. Wang, V. Dhir, An experimental investigation of multidimensional quenching of a simulated core debris bed, Nuclear Engineering and Design 110 (1) (1988) 61–72.

[19] G. Repetto, T. Garcin, S. Eymery, F. Fichot, Experimental program on debris reflooding (PEARL) – Results on PRELUDE facility, Nuclear Engineering and Design 264 (2013) 176–186.

[20] F. Fichot, A. Bachrata, G. Repetto, J. Fleurot, M. Quintard, Quenching of a highly superheated porous medium by injection of water, in: Journal of Physics: Conference Series, Vol. 395, IOP Publishing, 2012, p. 012144.

[21] R. Roser, B. Thonon, P. Mercier, Experimental investigations on boiling of n-pentane across a horizontal tube bundle: two-phase flow and heat transfer characteristics, International journal of refrigeration 22 (7) (1999) 536–547.

[22] L. Liao, Z.-H. Liu, Enhanced boiling heat transfer of the compact staggered tube bundles under sub-atmospheric pressures, Heat transfer engineering 28 (5) (2007) 444–450.

[23] L. Aprin, P. Mercier, L. Tadrist, Local heat transfer analysis for boiling of hydrocarbons in complex geometries: A new approach for heat transfer prediction in staggered tube bundle, International Journal of Heat and Mass Transfer 54 (19) (2011) 4203–4219.

[24] J. Broughton, P. Kuan, D. Petti, E. Tolman, A scenario of the three mile island unit 2 accident, Nuclear Technology 87 (1989) 34–53.

[25] R. McCardell, M. Russell, D. Akers, C. Olsen, Summary of TMI-2 core sample examinations, Nuclear Engineering and Design 118 (3) (1990) 441–449.

[26] E. Coryell, D. Akers, C. Allison, M. Carbonneau, R. Hobbins, J. Hohorst, S. Jensen, S. Modro, Summary of important results and SCDAP/RELAP5 analysis for OECD LOFT experiment LP-FP-2, Technical Report NUREG/CR-6160, Washington D.C., 1994.

[27] R. Manzel, C. Walker, EPMA and SEM of fuel samples from PWR rods with an average burn-up of around 100 MWd/kgHM, Journal of nuclear materials 301 (2) (2002) 170–182.